Photoproduction of η meson within a coupled-channels K-matrix approach

R. Shyam[1] and O. Scholten[2]

[1]*Saha Institute of Nuclear Physics, Kolkata 70064, India*

[2]*Kernfysisch Versneller Instituut, University of Groningen, 9747 AA, Groningen, The Netherlands*

(Dated: November 13, 2008)

Abstract

We investigate photoproduction of η mesons off protons and neutrons within a coupled-channels effective-Lagrangian method which is based on the K-matrix approach. The two-body final channels included are πN, ηN, ϕN, ρN, γN, $K\Lambda$, and $K\Sigma$. Non-resonant meson-baryon interactions are included in the model via nucleon intermediate states in the s- and u-channels and meson exchanges in the t-channel amplitude and the u-channel resonances. The nucleon resonances $S_{11}(1535)$, $S_{11}(1650)$, $S_{31}(1620)$, $P_{11}(1440)$, $P_{11}(1710)$, $\mathrm{P}_{13}(1720)$, $P_{33}(1232)$, $P_{33}(1600)$, $\mathrm{D}_{13}(1520)$, $D_{13}(1700)$, and $D_{33}(1700)$ are included explicitly in calculations. Our model describes simultaneously the available data as well on total and differential cross sections as on beam and target asymmetries. This holds for the $\gamma p \to \eta p$ reaction for photon energies ranging from very close to threshold to up to 3 GeV. The polarization observables show strong sensitivity to resonances that otherwise contribute only weakly to the total cross section. It is found that the pronounced bump-like structure seen in the excitation function of the $\gamma n \to \eta n$ cross section at γ energies around 1 GeV, can be explained by the interference effects of S_{11}, P_{11} and P_{13} resonance contributions.

PACS numbers: $13.60.Le$, $13.75.Cs$, $11.80.-m$, $12.40.Vv$

I. INTRODUCTION

It is well established that nucleons have a rich excitation spectrum which reflects their complicated multi-quark inner dynamics. The determination of properties of the nucleon resonances (e.g., their masses, widths, and coupling constants to various decay channels) is an important issue in hadron physics. This will provide the benchmark for testing the predictions of lattice quantum chromodynamics (LQCD) which is the only theory which tries to calculate these properties from first principles [1]. Even though, the requirement of computational power is enormous for their numerical realization, such calculations have started to provide results for nucleon properties for its ground as well as excited states [2, 3]. Furthermore, reliable nucleon resonance data are also important for testing the "quantum chromodynamics (QCD) based" quark models of the nucleon (see, *e.g.*, [4, 5]) and also the dynamical coupled-channels models of baryonic resonances [6].

Experimental determination of baryonic resonance properties proceeds indirectly by exciting the nucleon with the help of a hadronic or electromagnetic probe and performing measurements of their decay products (mesons and nucleons). The reliable extraction of nucleon resonance properties from such experiments is a major challenge. Description of intermediate-energy scattering is still too far away from the scope of the LQCD calculations. Therefore, at this stage the prevailing practice is to use effective methods to describe the dynamics of meson production reactions. Such methods include explicit baryon resonance states, whose properties are extracted by comparing the prediction of the theory with the experimental data [7, 8, 9, 10, 11, 12].

In order to determine resonance properties reliably from the experimental measurements one requires a model that can analyze the different reactions over the entire energy range using a single Lagrangian density that generates all non-resonance contributions from Born, u- and t-channel contributions without introducing new parameters. At the same time, the Lagrangian should also satisfy the symmetries of the fundamental theory (i.e. QCD) while retaining only mesons and baryons as effective degrees of freedom. Conformity with chiral symmetry is known to be important for low energy pion-nucleon physics.

A way to analyze simultaneously all reaction data for a multitude of observables in different reaction channels while respecting the constrains described above, is provided by a coupled-channels method within the K-matrix approach [13, 14, 15, 16, 17, 18]. This method

is attractive because it is based on an effective-Lagrangian framework that is gauge invariant and is consistent with chiral symmetry. It also provides a convenient way of imposing the unitarity constraint. This results from the Bethe-Saltpeter equation in the approximation where only the discontinuity part of the loop integral is retained i.e, the particles forming the loop are taken on the mass shell. The S matrix in this approach is unitary provided the K-matrix is taken to be real and Hermitian.

Alternatively, the dynamical coupled channels models within the Hamiltonian formalism have also been used to describe the meson-production reactions [19, 20, 21]. A relativistic chiral unitary approach based on a coupled-channels prescription has been used in Ref. [22] to calculate cross sections for η photoproduction. This reaction has also been studied in chiral perturbation theory [23] and in the chiral constituent-quark model [24].

In this paper we investigate photoproduction of the η meson which is the next lightest non-(open)strange member in the meson mass spectrum. This is a subject of considerable interest. It can be used to probe the $s\bar{s}$ component in the nucleon wave function [25]. There is also interest in measuring the rare decays of η mesons which could provide a new rigorous test of the standard model [26] or even of the physics beyond this. The nucleon resonance $N^*(1535)$ $[S_{11}(1535)]$ with spin-$\frac{1}{2}$, isospin-$\frac{1}{2}$, and odd parity, has a remarkably large ηN branching ratio. It lies only about 50 MeV above the $N\eta$ production threshold, and contributes dominantly to the photoproduction amplitude at energies close to threshold. Thus this reaction is an ideal tool to study the $N^*(1535)$ resonance which has been the subject of some debate recently (see, e.g., [27]). The attractive nature of the η-nucleon interaction may lead to the formation of bound (quasi-bound) η-nucleus states (see, e.g., [28, 29, 30, 31, 32]).

Photoproduction reactions provide a sensitive tool to study baryonic resonances. Apart from giving information which is complementary to that extracted from the studies of hadronic reactions, it gives access to additional information about the weakly excited resonances through the polarization observables [33]. The η meson has zero isospin (I), hence the ηN final states can only be reached via excitation of $I = \frac{1}{2}$ resonances (N^*). This is in contrast to the πN channel where both $I = \frac{1}{2}$ and $I = \frac{3}{2}$ intermediate states are possible. Thus even if a resonance has only a small coupling to the ηN channel, it is identified as a N* state.

With the advent of new high-duty-cycle electron accelerators and intense photon sources

with sophisticated detectors, a rich variety of very precise data have been accumulated on total and differential cross sections and beam and target asymmetries for η meson photoproduction off the free proton [34, 35, 36, 37, 38, 39, 40, 41, 42, 43, 44]. For a comprehensive review of the data up to 2003 and their interpretations, we refer to [45]. The eta-Maid [9] and partial wave analyses [46] of these data reveal that while the cross sections are dominated by the excitation of the $S_{11}(1535)$ resonance in the threshold region and by the $P_{13}(1720)$ resonance at higher photon energies, beam and target asymmetries are sensitive to the weakly excited $D_{13}(1520)$ and $P_{11}(1710)$ resonances via interference with the strongly excited ones.

Extensive measurements have also been performed for the η meson production on a deuterium target [35, 47, 48, 49, 50, 51]. These data have provided useful information on the isospin structure of electromagnetic excitations of the $S_{11}(1535)$ resonance and have led to the determination of the $\gamma n \to \eta n$ / $\gamma p \to \eta p$ cross-section ratio. An interesting observation of the data on the (quasi-free) neutron is that the corresponding excitation function of the total cross section shows a bump-like structure around photon energies of 1 GeV - such a bump is not seen in the proton case. This bump structure has been explained either in terms of the presence of a $D_{15}(1675)$ resonance with an unusually large branching ratio for its decay to the ηN channel [9] or due to coupled channels effects involving $S_{11}(1535)$, $S_{11}(1650)$ and $P_{11}(1710)$ resonances [52] within a coupled-channels effective Lagrangian model. In the latter approach, contributions of spin-$\frac{5}{2}$ resonances are found to be negligibly small. In an yet another explanation, it has been suggested that this bump may be a signal of the existence of a relatively narrow (width < 30 MeV) baryonic state with mass around 1.68 GeV [50, 53].

The main objective of this paper is to study photoproduction of η mesons on the bare proton and neutron for photon energies ranging from threshold to 3 GeV in a coupled-channels formalism which is based on the K-matrix approach. This is an effective Lagrangian model which is gauge invariant and obeys the low-energy theorem. We aim at describing simultaneously the data on total and differential cross sections and beam and target asymmetries. As described above the data base on η photoproduction has been enhanced appreciably during recent times. It is a challenge to any theoretical model to describe all the available data within one framework.

We would like to add that our work, in a way, supplements the coupled-channels effective-Lagrangian model calculations of this reaction presented within the Giessen model [12]. Although the two approaches are similar in physics contents, they differ in some details. An

important difference lies in the inclusion of reaction channels leading to states outside the model space. The Giessen model parameterizes the $2\pi N$ final state, as enters for example in the $\gamma N \to 2\pi N$ reaction, by an effective ξN state, where ξ is an isovector scalar meson with mass $m_\xi = 2m_\pi$. In our model the coupling to states outside the model space is taken into account by allowing for an energy dependent decay width to these states in the propagators for the different resonances. Another important difference lies in the choice of contact terms and form factors. As shown in Ref [16] contact terms in photo-induced reactions, which are magnetic in origin, are not important at low energies but have a considerable effect at higher energies. A more minor difference is that in the present calculation we have chosen to exclude spin-$\frac{5}{2}$ resonances from our study as their contributions are shown [52] to be almost negligible to η photoproduction in comparison to those of the dominant lower-spin states. Unlike the Giessen work we have not performed a full blown χ^2 fitting of all the available $\gamma N \to \eta N$ data. Rather, we have used the parameter set obtained in a previous work within our model [16, 18] and have made adjustments in some of them so as to describe the ηN channel.

Our paper is organized in the following way. An overview of our model is given in section II. This consists of a short discussion of the K-matrix formalism, the model space and the channels included, the Lagrangians and the form factors. Our results and a discussion thereof are presented in section III. Summary and conclusions of our work is presented in section IV.

II. DESCRIPTION OF THE MODEL

This work is based on an effective-Lagrangian model. The kernel in the K-matrix approach is built by using the effective Lagrangian which is given in Appendix A. We have taken into account contributions from (i) the nucleon Born term, (ii) t-channel exchanges of mesons, (iii) nucleon and resonance terms in the u-channel, and (iv) baryonic resonance in the s-channel (see Fig. 1). The sum of amplitudes (i), (ii) and (iii) is termed as the background contribution in the following. As is discussed below, this approach allows to account for coupled-channels effects while preserving many symmetries of a full field-theoretical method.

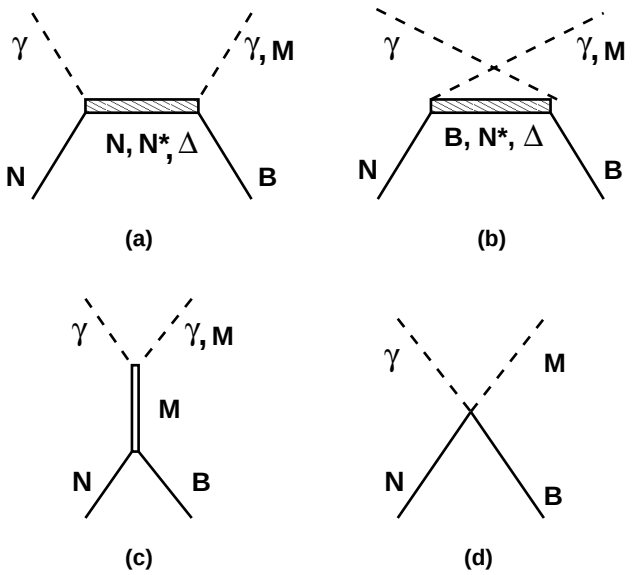

FIG. 1: [color online] Feynman diagrams included in this work. First row: s- and u-channel diagrams with propagating final state baryons ($B = N$, Λ, Σ) or intermediate state resonances (Δ, N^*). M stands for the mesons included in the model space. Second row: t-channel contributions with propagating asymptotic and intermediate mesons, and the contact term required by the gauge invariance.

A. K-matrix model

The coupled-channels (or re-scattering) effects are included in our model via the K-matrix formalism. In this section we present a short overview of this approach; a more detailed description can be found in Refs. [14, 16, 54, 55].

In the K-matrix formalism the scattering matrix is written as

$$\mathsf{T} = \frac{\mathsf{K}}{1 - i\mathsf{K}}\,. \tag{1}$$

It is easy to check, that the resulting scattering amplitude $S = 1+2i\mathsf{T}$ is unitary provided that K is Hermitian. The construction in Eq. (1) can be regarded as the re-summation of an infinite series of loop diagrams by making a series expansion,

$$\mathsf{T} = \mathsf{K} + i\mathsf{K}\mathsf{K} + i^2\mathsf{K}\mathsf{K}\mathsf{K} + \cdots\,. \tag{2}$$

The product of two K-matrices can be rewritten as a sum of different one-loop contributions (three- and four-point vertex and self-energy corrections) depending on the Feynman diagrams that are included in the kernel K. However, not the entire spectrum of loop corrections

TABLE I: Baryon states included in the calculation of the kernel with their coupling constants. The column labeled WD lists the decay width to states outside the model space. The columns labeled M and WD are in units of GeV. See text for a discussion on the signs of the coupling constants.

L_{IJ}	M	WD	$g_{N\pi}$	$g^1_{p\gamma}$	$g^2_{p\gamma}$	$g^1_{n\gamma}$	$g^2_{n\gamma}$	$g_{K\Lambda}$	$g_{K\Sigma}$	$g_{N\eta}$
N	0.939	0.0	13.47	—	—	—	—	12	8.7	0.85
Λ	1.116	0.0	—	—	—	—	—	—	—	—
Σ	1.189	0.0	—	—	—	—	—	—	—	—
$S_{11}(1535)$	1.525	0.0	0.6	−0.60	—	0.5	—	0.1	0.0	2.2
$S_{11}(1650)$	1.690	0.030	1.0	−0.45	—	−0.45	—	−0.1	0.0	−0.8
$S_{31}(1620)$	1.630	0.100	3.7	−0.12	—	−0.12	—	—	−0.8	—
$P_{11}(1440)$	1.520	0.200	5.5	0.65	—	0.65	—	0.0	−2.0	0.0
$P_{11}(1710)$	1.850	0.300	3.0	0.25	—	−0.8	—	0.0	−3.0	2.0
$P_{13}(1720)$	1.750	0.300	0.12	−0.75	0.25	−0.25	0.05	−0.035	0.0	0.12
$P_{33}(1230)$	1.230	0.0	1.7	−2.2	−2.7	−2.2	−2.7	—	0.0	—
$P_{33}(1600)$	1.855	0.150	0.0	−0.4	−0.6	−0.4	−0.6	—	0.55	—
$D_{13}(1520)$	1.515	0.050	1.2	2.6	2.5	2.6	2.5	2.0	0.0	1.2
$D_{13}(1700)$	1.700	0.090	0.0	−0.5	0.0	−0.5	0.0	0.0	0.3	−0.04
$D_{33}(1700)$	1.670	0.250	0.8	1.5	0.6	1.5	0.6	—	−3.0	—

present in a true field-theoretical approach, is generated in this way and the missing ones should be accounted for in the kernel. In constructing the kernel, care should be taken to avoid double counting. For this reason we include in the kernel tree-level diagrams only [Figs 1(a)-1(c)], modified with form-factors and contact terms [Fig. 1(d)]. The contact terms (or four-point vertices) ensure gauge invariance of the model and express model-dependence in working with form factors (see Section III). Contact terms and form factors can be regarded as accounting for loop corrections which are not generated in the K-matrix procedure, or for short-range effects which have been omitted from the interaction Lagrangian. Inclusion of both s- and u-channel diagrams [Figs 1(a) and 1(b), respectively] in the kernel insures the compliance with crossing symmetry.

To be more specific, the loop corrections generated in the K-matrix procedure include only those diagrams which correspond to two on-mass-shell particles in the loop [56, 57]. This is the minimal set of diagrams one has to include to ensure two-particle unitarity. Not included, thus, are all diagrams that are not two particle reducible. This excludes the $\gamma N \to 2\pi N$ channels from the realm of our model. In addition, only the convergent pole contributions i.e. the imaginary parts of the loop correction, are generated. The omitted real

parts are important to guarantee analyticity of the amplitude and may have complicated cusp-like structures at energies where other reaction channels open. In principle, these can be included as form factors as is done in the dressed K-matrix procedure [56, 58]. For reasons of simplicity we have chosen to work with purely phenomenological form factors in the present calculations. An alternative procedure to account for the real-loop corrections is offered by the approach of Ref. [59] which is based on the use of a Bethe-Saltpeter equation. This approach was recently extended to kaon production in Ref. [60]. Another possible approach is the one discussed in Ref. [61] which is based on an N/D expansion of the T matrix combined with a dispersion-integral approach.

The strength of the K-matrix procedure is that in spite of its simplicity, several symmetries are obeyed by it [54]. As was already noted the resulting amplitude is unitary provided that K is Hermitian, and it obeys gauge invariance provided the kernel is gauge-invariant. In addition, the scattering amplitude complies with crossing symmetry when the kernel is crossing symmetric. This property is crucial for a proper behavior in the low-energy limit [57, 62] of the scattering amplitude. Coupled-channels effects are automatically accounted for by this approach for the channels explicitly included into the K-matrix as the final states.

As a result of this channel coupling, the resonances generate widths which are compatible with their decays to channels included in the model space. For some resonances, such as the Δ and the $S_{11}(1535)$, this corresponds to their total width. Other resonances, particularly the high lying ones, may have important decay branches to states that are not included in the model basis. To account for this in our calculations, we have added an explicit dissipative part to the corresponding propagators. The magnitudes of these widths are equivalent to decay widths of the resonances to states outside of our model space.

The resonances which are taken into account in building the kernel are summarized in Table I. In the current work we limit ourselves to the spin-$\frac{1}{2}$ and spin-$\frac{3}{2}$ resonances as in this energy regime higher spin resonances are known [52] to give only a minor contribution to the ηN channel which is of primary interest here. Spin $\frac{3}{2}$ resonances are included with so-called gauge-invariant vertices which have the property that the coupling to the spin-$\frac{1}{2}$ pieces in the Rarita-Schwinger propagator vanish [56, 64]. We have chosen this prescription since it reduces the number of parameters as we do not have to deal with the off-shell couplings. The effects of these off-shell couplings can be absorbed in contact terms [65] which we prefer, certainly within the context of the present work.

TABLE II: Mass, spin, parity and isospin of the mesons which are included in the model. The rightmost column specifies in which reaction channels their t-channel contribution are taken into account.

Meson	M [GeV]	S^π	I	t-ch contributions
π	0.135	0^-	1	$(\gamma N \to \phi N)$, $(\pi N \to \rho N)$
K	0.494	0^-	$\frac{1}{2}$	$(\gamma N \to K\Lambda)$, $(\gamma N \to K\Sigma)$
ϕ	1.019	1^-	0	
η	0.547	0^-	0	$(\gamma N \to \phi N)$
ρ	0.770	1^-	1	$(\gamma N \to \pi N)$, $(\gamma N \to \eta N)$, $(K\Lambda \to K\Sigma)$, $(K\Sigma \to K\Sigma)$, $(N\pi \to K\Lambda)$, $(N\pi \to N\eta)$, $(N\pi \to N\pi)$
ω	0.781	1^-	0	$(N\gamma \to N\pi)$,$(N\gamma \to N\eta)$
σ	0.760	0^+	0	$(N\gamma \to N\phi)$, $(N\pi \to N\pi)$
K^*	0.892	1^-	$\frac{1}{2}$	$(N\gamma \to K\Lambda)$,$(N\gamma \to K\Sigma)$, $(K\Lambda \to N\eta)$, $(K\Sigma \to N\eta)$, $(N\pi \to K\Sigma)$

The masses of the resonances given in Table I are bare masses and they thus may deviate from the values given by the Particle Data Group [66]. Higher-order effects in the K-matrix formalism do give rise to a (small) shift of the pole-position with respect to the bare masses. The masses of very broad resonances, in particular the P_{11}, are not well determined - values lying in a broad range (typically a spread of the order of a quarter of the width) give comparable results. The width quoted in Table I corresponds to the partial width for decay to states outside our model space. The parameters as quoted in Table I are mostly unchanged as compared to those presented in previous calculations within this model [16, 18]. It should however, be noted that values of the coupling constants for the electromagnetic vertices in Ref. [18] were given after multiplying them (mistakenly) by a factor of 2. This has not been done in Table I. The t-channel contributions which are included in the kernel, are summarized in Table II.

In the present calculation all primary coupling constants to the nucleon have been chosen to be positive. In particular, the sign of $g_{NK\Lambda}$ deviates from the customary negative value [67]

(see Table I). In a calculation like ours and many of those cited in Ref. [67] this sign is undetermined. Changing the sign of all coupling constants involving a single Λ-field leaves the calculated observables invariant since it corresponds to a sign redefinition of this field. In weak decay the ratio of the vector to axial-vector coupling does correspond to an observable. The magnitudes of the couplings are within the broad range specified in [67].

B. Model space, channels included

To keep the model manageable and relatively simple, we consider only stable particles or narrow resonances in two-body final states which are important for η-meson photoproduction. The ΛK, ΣK, $N\phi$, $N\eta$ and $N\gamma$ are the final states of primary interest, and the $N\pi$ final state is included for its strong coupling to most of the resonances. Three-body final states, such as $2\pi N$, are not included explicitly for reasons of simplicity. Their influence on the width of resonances is taken into account by assigning an additional (energy dependent) width to them [14]. To investigate the effects of coupling to more complicated states, we have also included the $N\rho$ final state. As was shown in Ref. [16], inclusion of the ρ channel has a strong influence on the pion sector but only a relatively minor effect on Λ and Σ photoproduction.

The components of the kernel which couple the different non-electromagnetic channels are taken as the sum of tree-level diagrams, similar to what is used for the photon channels. For these other channels no additional parameters were introduced and they thus need no further discussion.

III. FORM-FACTORS & GAUGE RESTORATION

A calculation with Born contributions, without the introduction of form factors, strongly overestimates the cross section at higher energies. Inclusion of coupled-channels effects reduces the cross section at high energies; however not sufficiently to produce agreement with the experimental data, and one is forced to quench the Born contribution with form factors. There are two physical motivations for introducing form factors (or vertex functions) in our calculation. First of all, at high photon energies one may expect to become sensitive to the short-range quark structure of the nucleon. Because this physics is not included explicitly in

our model, we can only account for it through the introduction of phenomenological vertex functions. The second reason has to do with the intermediate-range effects because of meson-loop corrections which are not generated through the K-matrix formalism. Examples of these are given in Refs. [56, 58].

In our approach as well as that of Ref. [15], the form-factors are not known *a priori* and thus they introduce certain arbitrariness in the model. In the current paper we limit ourselves to dipole form-factors in s-, u-, and t-channels because of their simplicity,

$$F_m(s) = \frac{\lambda^2}{\lambda^2 + (s - m^2)^2} \,, \tag{3}$$

where m is the mass of the propagating particle and λ is the cut-off parameter. For ease of notation we introduce the subtracted form factors

$$\tilde{f}_m(s) = \frac{1 - F_m(s)}{s - m^2} \,, \tag{4}$$

where $F_m(s)$ is normalized to unity on the mass-shell, $F_m(m^2) = 1$, and $\tilde{f}_m(m^2)$ is finite.

However, only in the kaon sector we use a different functional form for the u-channel form-factors

$$H_m(u) = \frac{u\lambda^2}{\big(\lambda^2 + (u - m^2)^2\big)m^2}. \tag{5}$$

The argumentation for this different choice is presented in the discussion of the Σ-photoproduction results in Ref. [16]. Often a different functional form and cut-off values are introduced for t-channel form factors. Although this can easily be motivated, it introduces additional model dependence and increases the number of free parameters. To limit the overall number of parameters we have taken the same cut-off value ($\lambda = 1.2$ GeV^2, see Eq. (3)) for all form-factors except for Born contributions in kaon channels where we used $\lambda = 1.0$ GeV^2.

Inclusion of form-factors will in general break electromagnetic gauge-invariance of the model. Therefore, a gauge-restoration procedure should be applied. In Ref. [16], the implications of various gauge-restoration procedures was studied for the $\gamma p \to K\Sigma$ amplitude. It was observed that the gauge-invariance restoration procedure is model dependent which may give rise to strongly different Born contributions to the amplitude. Therefore, the choice of a procedure to be adopted is guided by its ability to describe the experimental data. It was found that the gauge-restoration procedure of Davidson and Workman [68] provided

the best description of the data on the $K\Sigma$ photoproduction. We have used this procedure in the present work also.

We note that fitting the pion-scattering and pion-photoproduction amplitudes fixes masses as well as pion- and photon-coupling constants for most of the resonances. This limits strongly the number of free parameters for the kaon-production channels.

IV. RESULTS AND DISCUSSIONS

Our main aim in this paper is to use the comprehensive data base of the η-meson production to check various ingredients and input parameters of our unitary coupled-channels field theoretic model of meson production in photon induced reactions on nucleons. The requirement of a simultaneous fit to data for a multitude of observables is expected to provide a strong constraint on the values of the model parameters. It is also likely to highlight the role of channel couplings in various regions of photon energies because several calculations of η-meson photoproduction reactions have neglected these effects [7, 9, 10, 46, 69, 70].

We emphasize however, that even the large experimental data base may not allow to fix the extracted parameters uniquely within the unitary coupled-channels effective-Lagrangian model [15]. This is due to the fact that it is necessary to include empirical form factors in the model to regularize the amplitudes at higher energies. These form factors require a gauge-invariance restoration procedure which involves ambiguities. Nevertheless, confronting the model with a large data base is expected to provide a means to overcome this problem.

The parameters in the model have been adjusted [18] to reproduce the Virginia Tech partial wave amplitudes of Arndt et al. [71]. In Fig. 2 we present a comparison of our calculated pion-nucleon S-, P-, and D-wave amplitudes for isospins $I = 1/2$ and $3/2$ channels with those of the FA08 single-energy partial wave amplitudes of Ref [71]. The corresponding results for pion photoproduction and the Compton scattering are given in Ref. [18]. We see that both real and imaginary parts of the pion-nucleon scattering amplitudes are described well although some differences start to show up at the upper limit of the energy range considered.

The data for η meson photoproduction consist of total and differential cross sections measured at CB-ELSA at Bonn [41, 42] on the proton, for photon energies ranging from 0.750 GeV to 3 GeV. These data, therefore, cover not only the entire resonance region

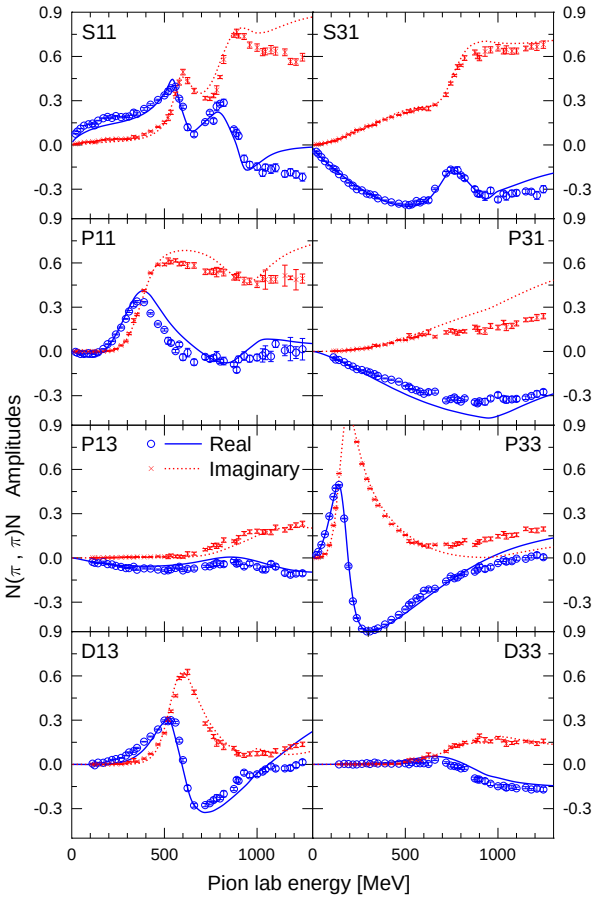

FIG. 2: [color online] The real (solid lines) and imaginary (dotted lines) pion-nucleon S-, P-, and D-wave amplitudes. The curves represent the results of our calculations while open circles and crosses are the results of Virginia Tech single-energy partial wave FA08 analysis [71].

but also the region where the background contributions (t-channel amplitudes mainly) are expected to be dominant. These data are consistent with the measurements reported by Mainz-TAPS [35], CLAS [39] and GRAAL [40, 44] collaborations where photon energies go up to 0.790 GeV, 1.95 GeV and 1.1 GeV, respectively. The data on beam asymmetry have been taken by the CB-ELSA group for photon energies in the range of 0.800 GeV to 1.4 GeV. In this case too there is an agreement (except for a single bin in photon energy) between these data and those of the GRAAL group [36, 44] where photon energies are in the range to 0.724 GeV to 1.472 GeV. One set of data on the target asymmetry (analyzing power) has already been reported in Ref. [37] and more measurements are planned by the CB-ELSA group.

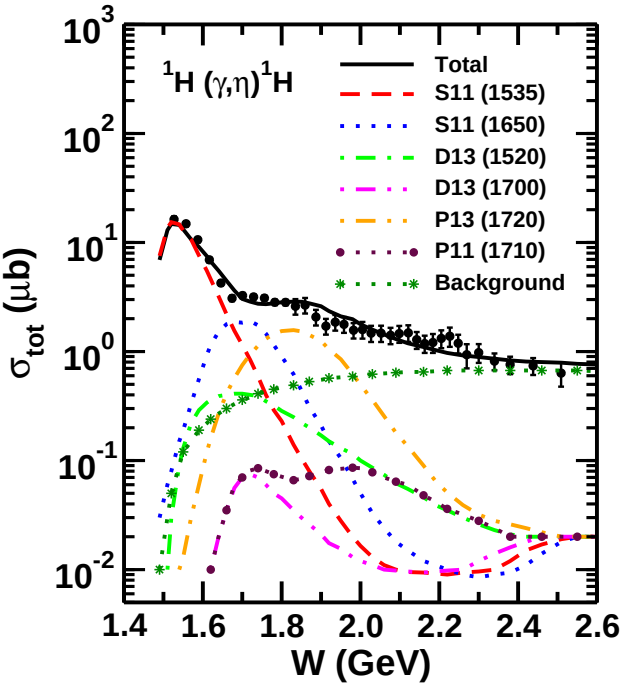

FIG. 3: [color online] Total cross section for the $\gamma p \to \eta p$ process as a function of γp invariant mass. The experimental data are taken from Ref. [41]. Contributions of resonances $S_{11}(1535)$, $S_{11}(1650)$, $P_{11}(1710)$,$P_{13}(1720)$, $D_{13}(1520)$, $D_{13}(1700)$ are shown by various curves as indicated in the figure. Also shown are the background contributions which consist of Born and u- and t-channel terms.

Data on η-meson photoproduction off the neutron are not as well developed and extensive as those on the proton due to the non-availability of free neutrons as targets. In most cases the photoproduction is measured on the neutron bound in the deuteron by performing experiments on the deuterium target. In this sense the corresponding cross sections are "quasi-free". Calculations done for the free neutron will have to be corrected for the Fermi motion and other nuclear effects before comparing them with the quasi-free production data. This procedure is not unique because of the prescription used in unfolding the recoil momentum of the "spectator" particle. Furthermore, quasi-free cross sections are also influenced by off-shell and final-state interaction effects. Nevertheless, quality data are now available for total and differential cross sections for η-meson photoproduction off the quasi-free neutrons [51]. This also includes the ratio of the total cross sections for this reaction on the neutron and the proton measured under identical conditions off the nucleon bound in the deuteron.

In Fig. 3, we show the contribution of various resonances to the total cross section for

the $\gamma p \to \eta p$ reaction which is plotted here as a function of the γp invariant mass W. The experimental data are taken from Ref. [41]. Since data of the various experimental collaborations are consistent with each other, we show the data of only one group (which span the maximum range of photon energy, E_γ) on this plot. From this figure it is apparent that the general features of the data are described reasonably well by our calculations in the entire range of beam energies where data are available. It should, however, be mentioned that our model slightly overpredicts (underpredicts) the data for W in the range of 1.85-1.95 GeV (2.18-2.25 GeV). Even the partial wave analysis fits to these data reported in Ref [41] show signs of underpredicting the cross section for $W \sim 1.85$-1.95.

We note that while contributions of the $S_{11}(1535)$ resonance dominate the cross sections from near threshold to W values of 1.7 GeV (corresponding to $E_\gamma \sim 1.1$ GeV), those of the $S_{11}(1650)$ and $P_{13}(1720)$ resonance are important for E_γ between 0.950 GeV to 1.28 GeV and 1.1 GeV to 2.2 GeV, respectively. In fact, omission of the $S_{11}(1650)$ resonance worsens the description of the data for E_γ in the range of 1.0-1.2 GeV. The non-negligible contribution of this resonance is consistent with the conclusions of Refs. [9, 52, 70]. However, this is in contrast to the partial-wave analysis results of Ref. [46]. We further note that magnitudes of the $D_{13}(1520)$, $D_{13}(1700)$ and $P_{11}(1710)$ resonances are comparatively small in the entire range of photon energies.

It should be remarked that at $W \sim 1.716$ GeV, there are some differences between the GRAAL [40] and ELSA [41] data - there is a bump in the former around this energy which is almost absent in the latter. The existence of a third S_{11} resonance with a mass of 1.712 GeV was suggested in Ref. [24] from the analysis of the preliminary GRAAL data. Very recently, calculations performed within a constituent quark model show that the inclusion of the third S_{11} resonance with a slightly higher mass of 1.730 GeV, improves the agreement with the differential cross section and beam asymmetry data at some angles [72]. We, however, have chosen not to include a third S_{11} resonance in this work which is in line with the calculations done in Refs [9, 52]. Anyhow, in principle it is straight forward to include this resonance into our analysis which we propose to do in a future study.

Total cross sections beyond 2 GeV are almost solely governed by the contributions of the background terms which are dominated by the t-channel diagrams. In this region all resonance contributions are small and comparable to each other. The vector meson (ρ and ω) exchange terms give the largest contribution to the t-channel amplitudes. The importance of

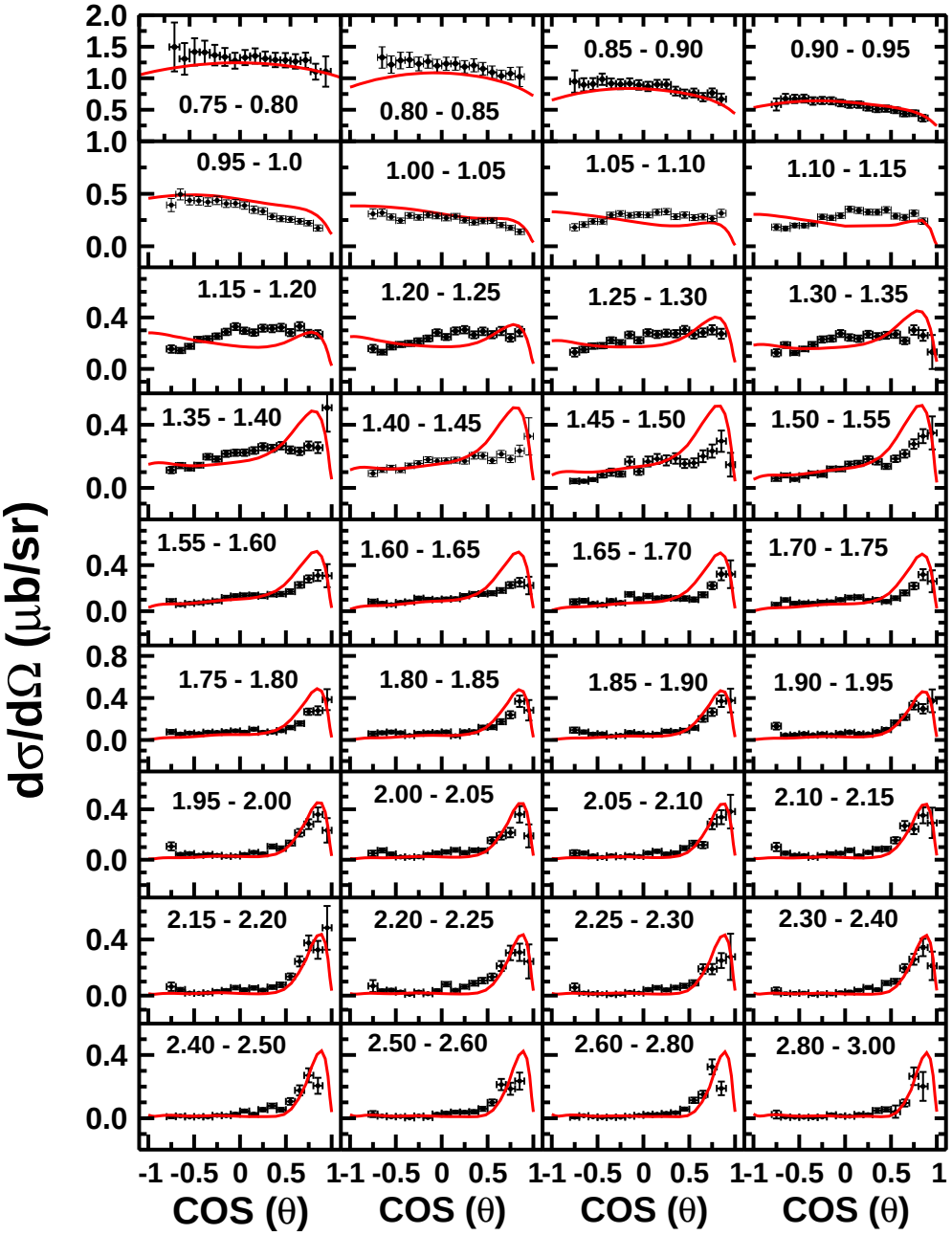

FIG. 4: [color online] Differential cross section for the $\gamma p \to \eta p$ process as a function of the cosine of the η c.m. angle for 36 photon energy bins. The energy bin is indicated in each graph in GeV. The experimental data are taken from Ref. [41].

this mechanism in the pion- and photon-induced ηN production, was already emphasized in the first coupled-channels model [73] for these reactions. There is some indication of a small bump like structure in the data for W around 2.2 GeV which might indicate the presence of a resonance in this region. The partial-wave analysis of these data [46] does include a

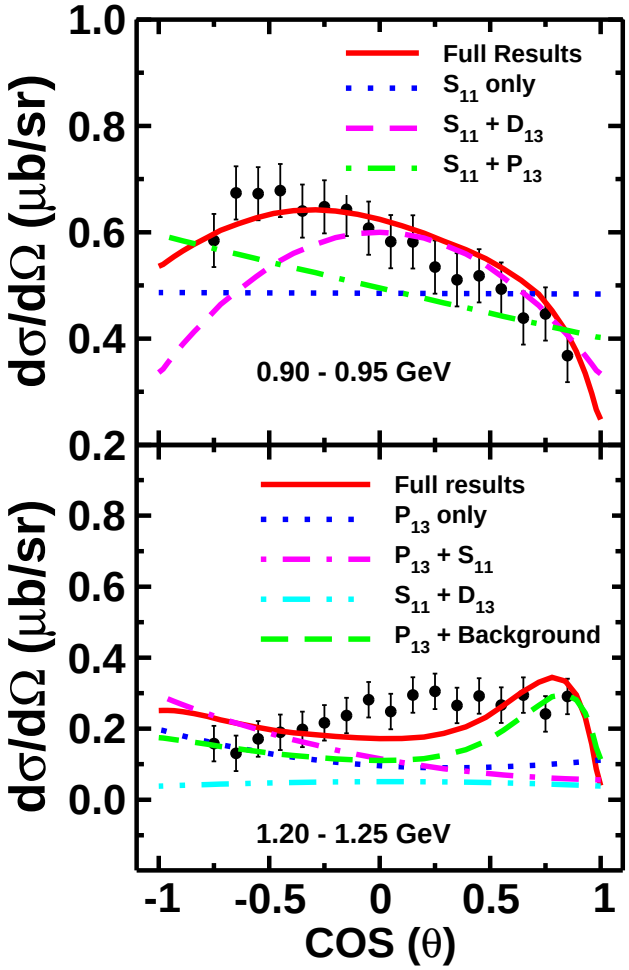

FIG. 5: [color online] Contributions of various resonance terms to the differential cross sections of the $\gamma p \to \eta p$ process as a function of the cosine of the η c.m. angle for photon energy bins of 0.90-0.95 GeV (upper panel) and 1.20-1.25 GeV (lower panel). Various curves are explained in the figure. The experimental data are from Ref. [41].

P_{13} resonance with mass 2.2 GeV and total width of 0.360 GeV in the fitting procedure. However, the existence of such a resonance is not yet to find a wider support (see, *e.g.*, Ref. [66]).

Differential cross sections (DCS) provide more valuable information about the reaction mechanism [74]. They reflect the quantum number of the excited state (baryonic resonance) when the cross section is dominated by it. DCS include terms that weigh the interference terms of various components of the amplitude with the outgoing η angles. Therefore, the structure of interference terms could highlight the contributions of different resonances in

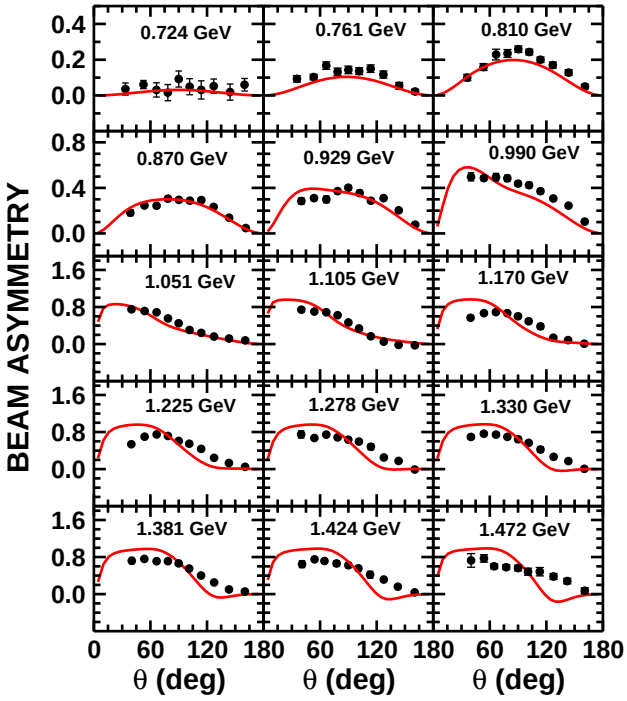

FIG. 6: [color online] Beam asymmetry for the $\gamma p \to \eta p$ reaction as a function of η c.m. angle for 15 photon energies. The experimental data are taken from Ref. [44].

different angular regions. For the $\gamma p \to \eta p$ reaction, DCS data exist for 36 photon energy bins in the range of 0.750 GeV to 3.0 GeV covering a wide range of η center of mass (c.m.) angles [41]. In Fig. 4, we compare the results of our calculations for the angular distributions with these data. We see that while our model describes the general trends of the data well in the complete energy region, a few specific details of the data are missed for some energy bins in the region of 1.0-1.60 GeV. For example, the curvature of the data is not reproduced by our calculations at middle angles for the photon energy bins lying between 1.0-1.25 GeV. There is a overprediction of the data at very forward angles for energy bins between 1.40-1.60 MeV.

Although individual contributions of the D_{13} and P_{13} resonances to the total cross section are rather small for $E_\gamma \leq 1.0$ GeV, their interference with the dominant S_{11} resonance amplitudes are vital for describing the experimental DCS data in this energy regime. We demonstrate this in Fig. 5 where we show individual contributions of various resonance terms to differential cross sections for photon energy bins of 0.900-0.950 GeV (upper panel) and 1.200-1.225 GeV (lower panel). For the lower energy bin, as expected, the contributions of

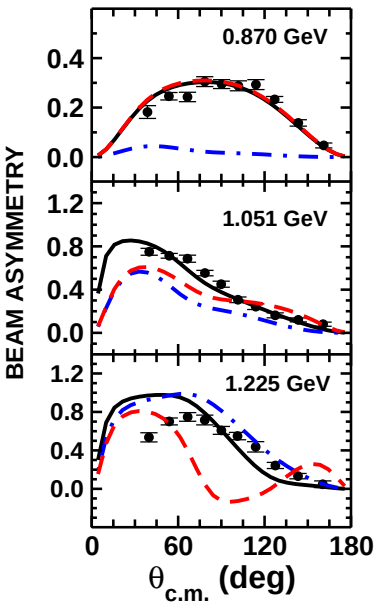

FIG. 7: [color online] Beam asymmetry for the $\gamma p \to \eta p$ reaction as a function of η c.m. angle for photon energies of 0.870 GeV, 1.051 GeV and 1.225 GeV. Solid lines show the full calculations where all the considered resonances and the background terms are included. The dashed and dashed-dotted curves are obtained when the $P_{13}(1720)$ and the $D_{13}(1520)$ resonances are omitted, respectively. The experimental data are taken from the Ref. [44].

S_{11} resonances are almost flat. However, inclusion of the D_{13} and P_{13} resonances together with S_{11} is crucial for describing the data for η angles below and above 90°, respectively. For the higher energy bin (lower panel), the S_{11} and D_{13} resonances do not contribute much at forward angles - here the P_{13} resonance and the background terms put together reproduce the shapes and magnitudes of the measured DCS. The forward peaking of the angular distributions beyond 1.8 GeV reflects the dominance of the t-channel meson exchange diagrams.

Polarization observables are more sensitive to the contributions of the resonances which are not dominant in the cross sections. Beam asymmetry (Σ_B) is the measure of the azimuthal anisotropy of a reaction yield relative to the linear polarization of the incoming photon. As compared to the cross-section data this observable is less sensitive to the $S_{11}(1535)$ resonance even at energies close to threshold. In Fig. 6, we compare results of our calculations for Σ_B with the experimental data of Ref. [44] which is available for 15 values of E_γ in the energy range of 0.724 GeV to 1.5 GeV. We note that there is an overall agree-

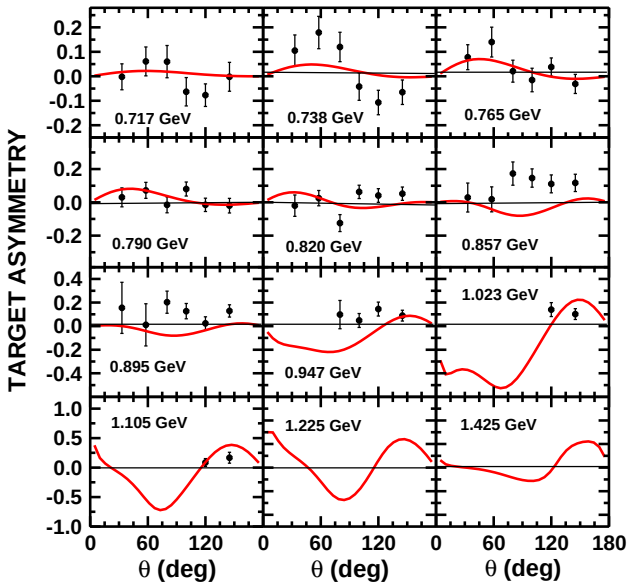

FIG. 8: [color online] Target asymmetry for the $\gamma p \to \eta p$ reaction as a function of η c.m. angle for various photon energies. Solid lines are the full calculations where all the considered resonances and the background terms are included. Experimental data are taken from the Ref. [37].

ment between our calculations and the experimental data in the complete range of photon energies.

The sensitivity of individual resonances to Σ_B is studied in Fig. 7 for three representative photon energies of 0.870 GeV, 1.051 GeV and 1.225 GeV. In each case the solid, dashed and dashed-dotted lines represent results of full calculations, and those obtained by ignoring contributions of the $P_{13}(1720)$ and $D_{13}(1520)$ resonances, respectively. We note that at the near threshold photon energy of 0.870 GeV, the $D_{13}(1520)$ resonance plays a very crucial role - the beam asymmetry goes from its maximum value of 0.35 to almost zero if this resonance is ignored. At the larger photon energy of 1.225 GeV, contributions of the $P_{13}(1720)$ resonance are important since the data can not be described without including them. At the intermediate photon energy (1.051 GeV) both the $D_{13}(1520)$ and the $P_{13}(1720)$ resonances are important. Our results for the higher photon energy (1.225 GeV) are in agreement with those of the Bonn-Gatchina partial wave analysis [46] as reported in Ref. [43] for the photon energy bin of (1.250 ± 0.050) GeV (in this reference the individual contributions of resonances are shown only for this bin). In contrast to this, in the eta-MAID analysis [43], Σ_B is insensitive to the P_{13} resonance at this value of E_γ. The crucial role of the $D_{13}(1520)$

resonance in describing the beam asymmetry at lower photon energies, was demonstrated already in Ref. [74]. Our work establishes this in conjugation with the description of the experimental data for the first time.

In Fig. 8, we have compared the results of our calculations for the target asymmetry (TA) with the corresponding experimental data reported in Ref. [37]. In general the predictions of our model are consistent with the trends seen in the data within error bars, except for E_γ between 0.857 GeV and 0.947 GeV where there is some incompatibility between data and our results. While at 0.857 GeV and 0.895 GeV the sign of the data is missed, at 0.947 GeV the sign change in the theoretical results occurs at somewhat higher angles in comparison to that of the data. In any case, the comparison between theory and data should be viewed in the light of the fact that the data have rather large error bars in both η angles and E_γ. It is worthwhile to note that our results show a qualitative similarity with those of Ref. [15] even though at certain photon energies energies some differences are noticeable between the two calculations.

In Fig. 9 we show TA as a function of E_γ for various η angles. In this figure we also show results obtained by omitting the P_{13} and D_{13} resonance contributions from the calculations (shown by dotted and dashed-dotted lines, respectively). Dashed curves show results where both these resonances have not been included. At lower energies for all angles, the interference effects of the P and D resonances with the dominant S_{11} ones are small. However, as energy increases, full results (solid lines) start deviating from those obtained by retaining only the S_{11} resonances, particularly for angles $> 33^\circ$. It is to be noted that interference effects of both the P_{13} and the D_{13} resonances with the S_{11} are important at higher energies and angles. In contrast to our study, the interference terms of the P resonances were not included in the analysis of Ref. [10]. In general our full results reproduce the trends seen in the data for all angles except for 80° and 100° where there are discrepancies between the two at higher photon energies.

The effects of channel couplings on the total cross section and beam asymmetry are studied in Figs. 10 and 11, respectively. In Fig. 10, we compare the results of full coupled channel calculations for the total cross section of the $\gamma p \to \eta p$ reaction (solid line) with those obtained by switching off the channel coupling effects (this will be referred as NCC) (dashed line). Full calculations are the same as those shown in Fig. 3. In the NCC case, the amplitudes of various processes are simply added together, ignoring the modifications

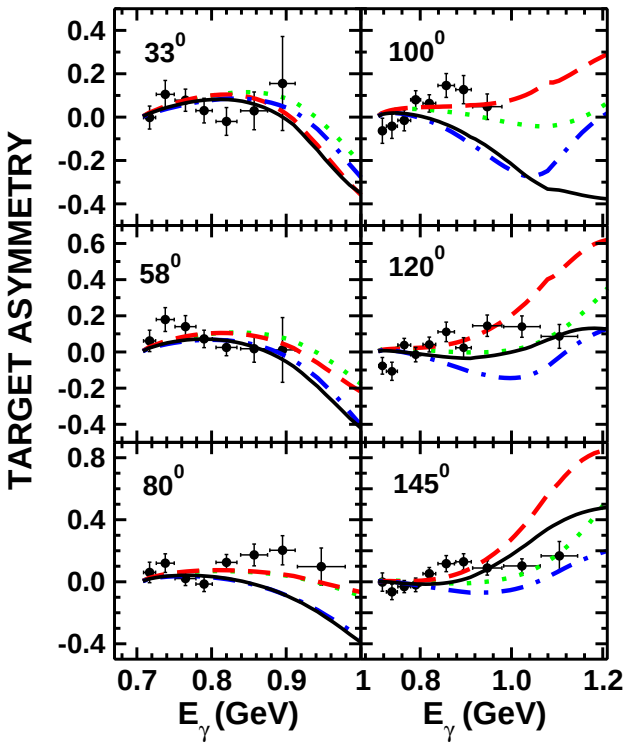

FIG. 9: [color online] Target asymmetry for the $\gamma p \to \eta p$ reaction as a function of photon energy for η c.m. angles of 33°, 58°, 80°, 100°, 120°, 145°. Solid lines show full results (as in Fig. 8) while dotted and dashed-dotted curves are obtained when P_{13} and D_{13} resonances are omitted from the calculations, respectively. The dashed curves result when both the P_{13} and the D_{13} resonances are excluded. The experimental data are taken from [37].

to the widths of the resonances introduced by the channel couplings. We notice that for W $>$ 1.8 GeV the differences between the full and the NCC results are very small. However, at lower energies, the channel-coupling effects are large and are crucial for describing the data. In fact, at some energies, the resonance propagators can develop poles in the absence of channel couplings. Thus modifications introduced to the widths of the resonances due to channel couplings are indeed vital for reproducing the energy dependence of the experimental cross sections.

In Fig. 11, we show the effect of channel coupling on the beam asymmetry Σ_B as a function of the η c.m. angle for various photon energies. In this case too, we notice that channel coupling effects are vital for describing the data at lower photon energies. For $E_\gamma <$ 1.225 GeV, the Σ_B in the NCC case are generally smaller and may even have wrong signs as

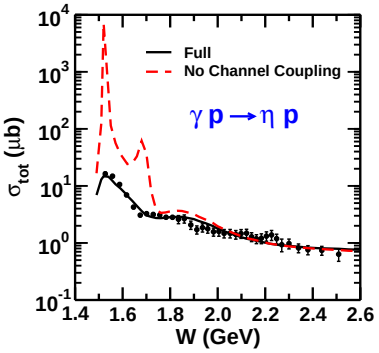

FIG. 10: [color online] Effect of channel coupling on the total cross section for the $\gamma p \to \eta p$ reaction as a function of γp invariant mass. The experimental data are taken from Ref. [41]. The solid line represents the results of the full coupled-channel calculations (same as that in Fig. 3) while the dashed line shows the one where channel coupling is switched off.

compared to those obtained in the full model. Thus channel coupling effects are extremely important in describing the magnitudes and the relative signs of the beam asymmetry data. The reason for this lies in the fact that polarization observables are generally very sensitive to the imaginary parts of the amplitudes which are governed by coupling to other channels via the optical theorem.

For the excitation of an isospin-$\frac{1}{2}$ resonance, both isoscalar and isovector components of the photon can contribute. In order to get information about the amplitudes corresponding to these components, data are needed for η-meson photoproduction off the neutron together with that off the proton. The non-existence of the free neutron target has prompted the use of a deuteron target to get information about the $\gamma n \to \eta n$ reaction. However, experiments on the deuteron provide information about the quasi-free production as the reaction takes place on the neutron bound in the deuteron where the Fermi motion of the nucleon inside the deuteron strongly influences the kinematics of the process.

The TAPS collaboration has studied the quasi-free η production off the neutron for E_γ ranging from threshold upto 0.820 GeV [49]. They have reported a constant ratio of 2/3 for $\gamma n \to \eta n$ and $\gamma p \to \eta p$ reactions at these near threshold energies. At the GRAAL facility both quasi-free production reactions have been explored simultaneously in the same experimental run with E_γ going upto 1.6 GeV [50]. They have reported a larger value for this ratio. Very recently, at the Bonn ELSA facility, simultaneous measurements have been performed for these reactions for incident photon energies being as large as 2.5 GeV [51].

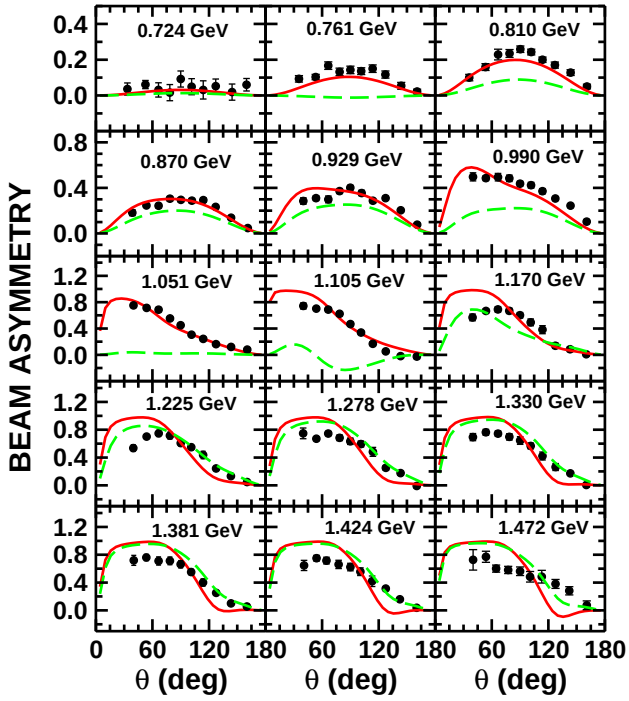

FIG. 11: [color online] Effect of channel coupling on the beam asymmetry for the $\gamma p \to \eta p$ reaction as a function of η c.m. angle for photon energies as indicated in each graph. Full coupled channel (same as that in Fig. 6) and no channel couplings results are shown by solid and dashed lines, respectively. The experimental data are taken from Ref. [44].

In this experiment data have been taken for angular distributions and total cross sections of the two reactions. The excitation function for η-meson photoproduction off the (quasi-free) neutron shows a pronounced bump-like structure at the invariant mass of 1.68 GeV (corresponding to $E_\gamma \approx 1.1$ GeV). A similar structure was also seen in the GRAAL data [50]. On the other hand, such a structure is not seen in the reaction off the proton (see Fig. 3).

As described earlier, this structure has been interpreted in altogether different ways by different authors. We believe that before going for more exotic explanations, conventional mechanisms for η photoproduction on both the neutron and the proton should first be investigated in detail. Since our model provides a reasonable description of both cross section and polarization data for the $\gamma p \to \eta p$ reaction, it is natural to use it to describe the $\gamma n \to \eta n$ data as well. This will help in determining the neutron helicity amplitudes of the relevant resonances.

In Fig. 12, we present our results for the total cross sections of the $\gamma p \to \eta p$ and $\gamma n \to \eta n$

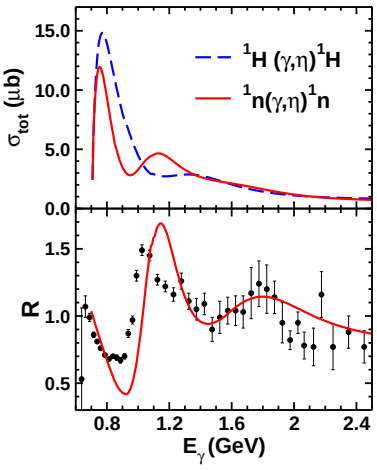

FIG. 12: [color online] (Upper Panel) Total cross sections (σ_{tot}) for $\gamma p \to \eta p$ (dashed line) and $\gamma n \to \eta n$ (full line) reactions as a function of incident photon energy. The former is the same as that shown by full line in Fig. 3. (Lower Panel) The ratio R of total cross sections of the $\gamma n \to \eta n$ and $\gamma p \to \eta p$ reactions as a function of photon energy. The data points shown in the lower panel have been taken from the Ref. [51].

reactions (upper panel) and for their ratio (R) (lower panel) using the helicity couplings for resonances as shown in Table I. We note that the value of the ratio $g_{n\gamma}/g_{p\gamma}$ is -0.8 for the $S_{11}(1535)$ resonance which is in agreement with the results of the combined theoretical studies of the $\gamma p \to \eta p$ and the $\gamma n \to \eta n$ reactions [9, 11, 52, 73, 75] and also with those extracted from the experimental data on the ratio of the two cross sections [49, 51]. In our study the helicity couplings of the neutron and the proton on the $S_{11}(1650)$ and $D_{13}(1520)$ resonances are the same. However, for the $P_{13}(1720)$ and the $P_{11}(1710)$ resonances they differ from each other which was also the case in Ref. [52].

We have not put the experimental data in the upper panel of Fig. 12 because for a comparison between theory and the data on the quasi-free η production, Fermi folding of our calculated cross sections will have to be performed in a way similar to that implemented in the extraction of the experimental data. However, in the lower panel we do show the data which are taken from Ref. [51]. We see that our calculations are consistent with the experimental observation of a bump-like structure around a photon energy of 1.1 GeV. Furthermore, yet another (rather broad) bump like structure is seen in the measured R at the photon energy of about 1.8 GeV. Our calculations are compatible with this structure

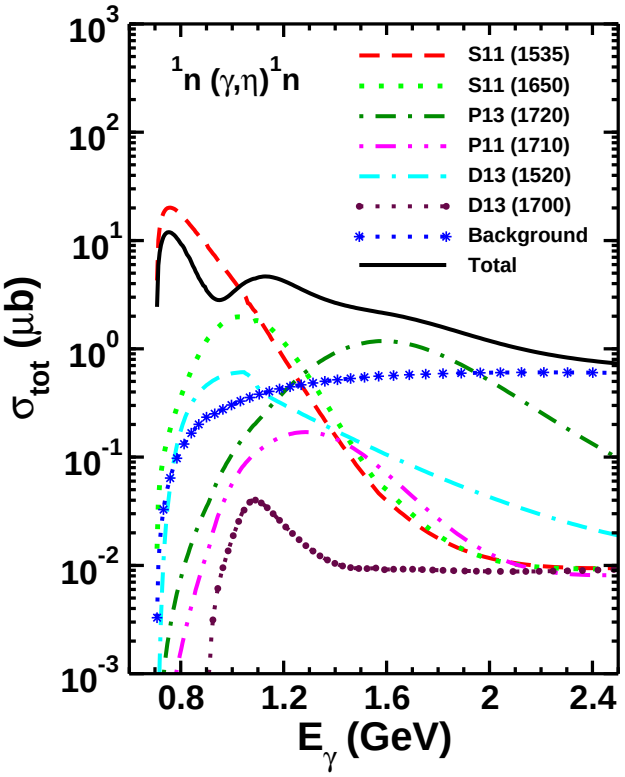

FIG. 13: [color online] Total cross section for the $\gamma n \to \eta n$ reaction as a function of incident photon energy. Contributions of the $S_{11}(1535)$, $S_{11}(1650)$, $P_{11}(1710)$,$P_{13}(1720)$, $D_{13}(1520)$, $D_{13}(1700)$ resonances are shown by various curves as indicated in the figure. Also shown are the background contributions.

as well. Thus, interference effects of mostly $S_{11}(1535)$, $S_{11}(1650)$, $P_{11}(1710)$, and $P_{13}(1720)$ resonances within a coupled channel approach can lead to the bump-like structures in the excitation function of η photoproduction off the neutron around photon energies of 1.1 GeV. They also lead to such structures in the neutron to proton cross-section ratio. The structures seen in our calculations are somewhat more pronounced than those observed in Ref. [52] where they result from similar interference effects.

The magnitude of the second peak seen in the total cross section of the $\gamma n \to \eta n$ reaction, is very sensitive to the values of the neutron helicity amplitudes of the S_{11}, $P_{11}(1710)$ and $P_{13}(1720)$ resonances. In Fig. 13, we show the contributions of various resonant states to the total cross section of this reaction. We note that in the region of the second peak, the main contributing resonances are $S_{11}(1535)$, $S_{11}(1650)$, $P_{13}(1720)$, $P_{11}(1710)$ and $D_{13}(1520)$. Therefore, the comparison of the calculations (with Fermi folding) with the data on the total

production cross section of this reaction will provide a check of the corresponding helicity amplitudes. Another interesting aspect of this figure is that there is a strong negative interference among the resonances at lower photon energies. In this region the $S_{11}(1535)$, $S_{11}(1650)$, and $D_{13}(1520)$ resonances are most relevant. Therefore, the data can be used to get further constraints on the helicity amplitudes of these three resonances.

As noted in case of the $\gamma p \to \eta p$ reaction, the differential cross sections provide a more stringent constraint on the contributions of even those resonances which participate only weakly in the total cross section. Data are also reported in Ref. [51] on differential cross sections of the $\gamma n \to \eta n$ reaction. In Fig. 14, we show results of our calculations for differential cross sections of this reaction at several photon energies. We have not put the data points in this figure as a meaningful comparison between calculations and the data would require the Fermi folding of the theoretical results as is stated before. However, some features of our results are worth noticing. For $E_\gamma \leq 0.900$ GeV there is a shape inversion in the angular distribution as compared to that observed in the case of the $\gamma p \to \eta p$ reaction at similar values of E_γ. This is consistent with the trend seen in the data. For $E_\gamma = 1.0$ GeV also similar inversion effect is present in the data except for the peaking in the forward direction. Our calculations also have this feature. For photon energies higher than this, angular distributions are of similar shapes for the two reactions due to the dominance of the t-channel contributions in both the cases.

V. SUMMARY AND CONCLUSIONS

In this paper we investigated the photoproduction of η meson off nucleons within a coupled-channels effective-Lagrangian approach which is based on the K-matrix method. Unitarity effects are correctly taken into account, since all important final channels (consisting of two-body systems πN, ηN, ϕN, ρN, γN, $K\Lambda$, and $K\Sigma$) are included in the K-matrix kernel. We build this kernel by using effective Lagrangians for the Born, u-channel, t-channel, and spin-$\frac{1}{2}$ and spin-$\frac{3}{2}$ resonance contributions. Thus, the background contributions are generated consistently and crossing symmetry is obeyed. The advantage of a full coupled-channel calculation is that it allows for the simultaneous calculation of observables for a large multitude of reactions with considerably fewer parameters than would be necessary if each reaction channel were fitted separately. More importantly, the implementation

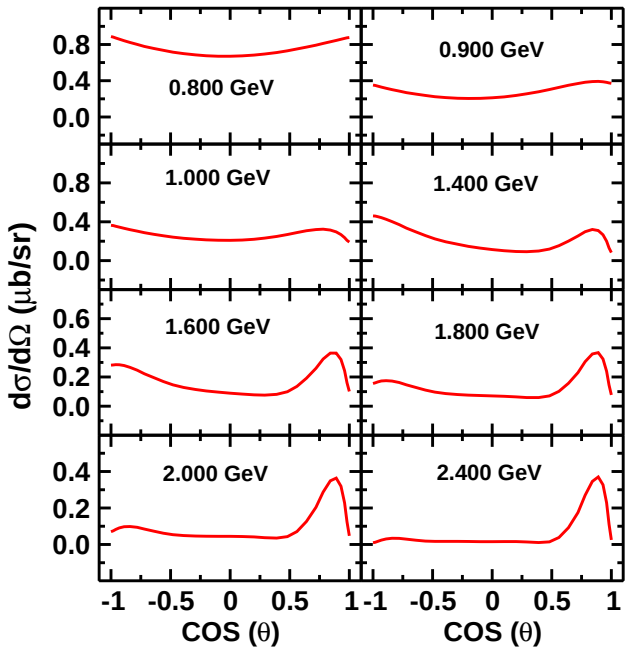

FIG. 14: [color online] Differential cross section for the $\gamma n \to \eta n$ reaction as a function of the cosine of the η c.m. angle at several photon energies indicated in each box.

of unitarity ensures that the imaginary parts of the amplitudes are compatible with the cross sections for other channels.

We showed that it is essential to use a full coupled-channels approach to describe the meson-production reactions. The effects of channels coupling are not merely a smooth change of the energy dependence of the cross sections. In their absence, they can acquire structures that might be misinterpreted as resonances. The polarization observables are also strongly affected by these effects where omitting channels coupling leads to wrong signs.

For η photoproduction off the proton, our model provides a reasonable description of the experimental data on total and differential cross sections as well beam and target asymmetries for photon energies ranging from threshold to up to 3 GeV. The previous effective Lagrangian based coupled-channels calculations of this reaction were restricted to photon energies below 2 GeV. We showed that the data on differential cross sections, and beam and target asymmetries are very sensitive to contributions of resonances which contribute only weakly to the total cross sections. For these observables, the interference of these resonances with the dominant $S_{11}(1535)$ amplitudes is vital for describing the data even at lower photon energies.

The second peak seen in the excitation function of the total cross section for η photoproduction off the neutron at photon energies around 1.1 GeV can be explained by the interference effects of the $S_{11}(1535)$, $S_{11}(1650)$, $P_{11}(1710)$ and $P_{13}(1720)$ resonances - there is no need to introduce an exotic narrow resonance state. We find that the ratio of the neutron to proton helicity amplitudes for the $S_{11}(1535)$ resonance has to be $\approx$ -0.8 in order to get the second peak in the total cross section as seen in the data. Our calculations are also compatible with the broad bump-like structures observed at photon energies around 1.1 GeV and 1.8 GeV in the ratio of total cross sections of η photoproduction off the neutron and the proton.

VI. ACKNOWLEDGMENTS

One of us (R.S.) acknowledges support from a visitors grant from the Dutch Organization for Scientific Research (NWO) during his stay at KVI.

APPENDIX A: EFFECTIVE LAGRANGIANS

We list here the effective Lagrangians for various vertices. p, k, $p\prime$ and $-q$ represent four momenta of the initial nucleon, final meson, final nucleon and photon, respectively. We assume that meson momenta are directed into the vertex, so that energy momentum conservation reads as $p + k = p\prime - q$.

For the nucleon vertices the following couplings were used

$$
\begin{aligned}
\mathcal{L}_{NN\pi} &= ig_{NN\pi}\bar{\Psi}_N \frac{(\chi\boldsymbol{\varphi}_\pi + i\partial\!\!\!/\boldsymbol{\varphi}_\pi/2m_N)\cdot\boldsymbol{\tau}}{\chi+1}\gamma_5\Psi_N \\
\mathcal{L}_{NN\eta} &= ig_{NN\eta}\bar{\Psi}_N \frac{\chi\varphi_\eta + i\partial\!\!\!/\varphi_\eta/2m_N}{\chi+1}\gamma_5\Psi_N \\
\mathcal{L}_{NN\sigma} &= -g_{NN\sigma}\bar{\Psi}_N\varphi_\sigma\Psi_N \\
\mathcal{L}_{NN\rho} &= -g_{NN\rho}\bar{\Psi}_N\left(\gamma_\mu\boldsymbol{\varphi}^\mu_\rho + \frac{\kappa_\rho}{2m_N}\sigma_{\mu\nu}\partial^\nu\boldsymbol{\varphi}^\mu_\rho\right)\cdot\boldsymbol{\tau}\Psi_N \\
\mathcal{L}_{NN\omega} &= -g_{NN\omega}\bar{\Psi}_N\left(\gamma_\mu\varphi^\mu_\omega + \frac{\kappa_\omega}{2m_N}\sigma_{\mu\nu}\partial^\nu\varphi^\mu_\omega\right)\Psi_N \\
\mathcal{L}_{NN\phi} &= -g_{NN\phi}\bar{\Psi}_N\left(\gamma_\mu\varphi^\mu_\phi + \frac{\kappa_\phi}{2m_N}\sigma_{\mu\nu}\partial^\nu\varphi^\mu_\phi\right)\Psi_N \\
\mathcal{L}_{NN\gamma} &= -e\bar{\Psi}_N\left(\frac{1+\tau_0}{2}\gamma_\mu A^\mu + \frac{\kappa_\tau}{2m_N}\sigma_{\mu\nu}\partial^\nu A^\mu\right)\Psi_N \\
\mathcal{L}_{NN\gamma\varphi} &= -e\frac{g_{NN\phi}}{2m_N}\bar{\Psi}_N\gamma_5\gamma_\mu[\boldsymbol{\tau}\times\boldsymbol{\varphi}]A^\mu\ .
\end{aligned}
\tag{A1}
$$

The parameter χ controls the admixture of pseudoscalar and pseudovector components in the corresponding Lagrangian. Its value is taken to be 0.5. This value was obtained in our previous study of photoproduction of associated strangeness [16] and has been held fixed in the study of all other reactions within our model. Nucleon spinors are depicted by Ψ and meson fields by φ. The magnetic moments are represented by κ. $\mathcal{L}_{NN\gamma\varphi}$ generates the seagull or the contact term diagrams. We have followed the notations of Ref. [76].

The Lagrangians for the meson vertices are

$$
\begin{aligned}
\mathcal{L}_{\rho\pi\pi} &= -g_{\rho\pi\pi}\boldsymbol{\varphi}_{\rho_\mu}\cdot(\boldsymbol{\varphi}_\pi\times\overleftrightarrow{\partial^\mu}\boldsymbol{\varphi}_\pi)/2 \\
\mathcal{L}_{\gamma\pi\pi} &= e\varepsilon_{3ij}A_\mu(\varphi_{\pi_i}\overleftrightarrow{\partial^\mu}\varphi_{\pi j}) \\
\mathcal{L}_{\rho\gamma\pi} &= e\frac{g_{\rho\gamma\pi}}{m_\pi}\boldsymbol{\varphi}_\pi\cdot\left(\varepsilon_{\mu\nu\rho\sigma}(\partial^\rho A^\mu)(\partial^\sigma\boldsymbol{\varphi}_\rho{}^\nu)\right) \\
\mathcal{L}_{\omega\gamma\pi} &= e\frac{g_{\omega\gamma\pi}}{m_\pi}\varphi_{\pi^0}\left(\varepsilon_{\mu\nu\rho\sigma}(\partial^\rho A^\mu)(\partial^\sigma\omega^\nu)\right) \\
\mathcal{L}_{\phi\gamma\pi} &= e\frac{g_{\phi\gamma\pi}}{m_\pi}\boldsymbol{\varphi}_{\pi^0}\left(\varepsilon_{\mu\nu\rho\sigma}(\partial^\rho A^\mu)(\partial^\sigma\phi^\nu)\right) \\
\mathcal{L}_{\phi\gamma\eta} &= e\frac{g_{\phi\gamma\eta}}{m_\pi}\varphi_\eta\left(\varepsilon_{\mu\nu\rho\sigma}(\partial^\rho A^\mu)(\partial^\sigma\varphi_\phi^\nu)\right) \\
\mathcal{L}_{\rho\gamma\eta} &= e\frac{g_{\rho\gamma\eta}}{m_\pi}\varphi_\eta\left(\varepsilon_{\mu\nu\rho\sigma}(\partial^\rho A^\mu)(\partial^\sigma\varphi_{rho^0}{}^\nu)\right) \\
\mathcal{L}_{\rho\gamma\sigma} &= e\frac{g_{\rho\gamma\sigma}}{m_\rho}(\partial^\mu\varphi_{\rho^\nu}\partial_\mu A_\nu-\partial^\mu\varphi_{\rho^\nu}\partial_\nu A_\mu) \\
\mathcal{L}_{\rho\rho\gamma} &= 2e\big(A^\mu(\partial_\mu\varphi_{\rho_\nu})\tau_0\varphi_\rho{}^\nu-(\partial^\nu A^\mu)\varphi_{\rho_\nu}\tau_0\varphi_{\rho_\mu} \\
&\quad +(\partial^\nu A^\mu)\varphi_{\rho_\mu}\tau_0\varphi_{\rho_\nu}\big) \\
\mathcal{L}_{\phi\mathsf{K}\mathsf{K}} &= -ig_{\phi\mathsf{K}\mathsf{K}}\bar{\boldsymbol{\varphi}}_\mathsf{K}\overleftrightarrow{\partial^\mu}\boldsymbol{\varphi}_\mathsf{K})\phi_\mu \\
\mathcal{L}_{\eta\mathsf{K}^*\mathsf{K}} &= -ig_{\eta\mathsf{K}\mathsf{K}^*}\boldsymbol{\varphi}_\mathsf{K}\overleftrightarrow{\partial^\mu}\varphi_\eta\bar{\boldsymbol{\varphi}}_{\mathsf{K}^*\mu} \\
\mathcal{L}_{\pi\mathsf{K}^*\mathsf{K}} &= -ig_{\pi\mathsf{K}\mathsf{K}^*}\bar{\boldsymbol{\varphi}}_\mathsf{K}\overleftrightarrow{\partial^\mu}\boldsymbol{\varphi}_\pi\cdot\boldsymbol{\tau}\boldsymbol{\varphi}_{\mathsf{K}^*\mu} \\
\mathcal{L}_{\rho\pi\eta} &= -ig_{\rho\pi\eta}(\varphi_\eta\overleftrightarrow{\partial^\mu}\boldsymbol{\varphi}_\pi)\boldsymbol{\varphi}_{\rho_\mu} \\
\mathcal{L}_{\mathsf{K}^*\mathsf{K}^0\gamma} &= \frac{g_{\mathsf{K}^*\mathsf{K}\gamma}}{m_\pi}\bar{\boldsymbol{\varphi}}_{\mathsf{K}^0}\left(\varepsilon_{\mu\nu\rho\sigma}(\partial^\rho A^\mu)(\partial^\sigma\boldsymbol{\varphi}_{\mathsf{K}^*}^\nu)\right) \\
\mathcal{L}_{\mathsf{K}^*\mathsf{K}^\pm\gamma} &= \frac{g_{\mathsf{K}^*\mathsf{K}\gamma}}{m_\pi}\bar{\boldsymbol{\varphi}}_{\mathsf{K}^\pm}\left(\varepsilon_{\mu\nu\rho\sigma}(\partial^\rho A^\mu)(\partial^\sigma\boldsymbol{\varphi}_{\mathsf{K}^*}^\nu)\right)\ .
\end{aligned}
\tag{A2}
$$

The coupling constants entering into Eqs. (A.1) and (A.2) together with baryon magnetic moments are listed in Table III.

For the S_{11}, S_{31},P_{11} and $P_{3,1}$ resonances the hadronic couplings are written as

$$
\mathcal{L}_{\varphi NR_{1/2}} \;=\; -g_{\varphi NR}\bar{\Psi}_R[\chi i\Gamma\varphi+(1-\chi)\frac{1}{M}\Gamma\gamma_\mu(\partial^\mu\varphi)]\Psi_N+\text{H.c.}, \tag{A3}
$$

where $M = (m_R \pm m_N)$, with upper sign for even parity and lower sign for odd parity resonance. The operator Γ is γ_5 and unity for even and odd parity resonances, respectively. For isovector mesons, φ in Eq. (A.3) needs to be replaced by $\boldsymbol{\tau}\cdot\boldsymbol{\varphi}$ for isospin-$\frac{1}{2}$ resonances and by $\mathbf{T}\cdot\boldsymbol{\varphi}$ otherwise.

The corresponding electromagnetic couplings are

$$
\mathcal{L}_{\gamma NR_{1/2}} \;=\; -eg_1\bar{\Psi}_R\frac{\Gamma}{4m_N}\sigma_{\mu\nu}\Psi_N F^{\mu\nu}+H.c., \tag{A4}
$$

TABLE III: Parameters summary table

$g_{NN\pi}$	13.47	$g_{NN\eta}$	0.85
$g_{NN\sigma}$	10.0	$g_{NN\rho}$	-2.2
$g_{NN\omega}$	-3.0	$g_{NN\phi}$	-0.0
$g_{N\Lambda\mathsf{K}}$	12.0	$g_{N\Sigma K}$	8.6
$g_{N\Lambda\mathsf{K}^*}$	-1.7	$g_{N\Sigma K^*}$	0.0
$g_{\Sigma\sigma\rho}$	-10.0	$g_{\Sigma\Lambda\rho}$	10.0
$g_{\phi\mathsf{K}\mathsf{K}}$	-4.5	$g_{\rho\mathsf{K}\mathsf{K}}$	-3.0
$g_{\pi\mathsf{K}\mathsf{K}^*}$	-3.26	$g_{\eta\mathsf{K}\mathsf{K}^*}$	-3.2
$g_{\rho\pi\pi}$	6.0	$g_{\rho\pi\eta}$	0.0
$g_{\rho\pi^0\gamma}$	-0.12	$g_{\rho\pi^\pm\gamma}$	-0.10
$g_{\rho\eta\gamma}$	-0.21	$g_{\omega\eta\gamma}$	-0.12
$g_{\omega\pi\gamma}$	0.32	$g_{\rho\sigma\gamma}$	12.0
$g_{\phi\pi\gamma}$	0.018	$g_{\phi\eta\gamma}$	0.096
κ_p	1.79	κ_n	-1.91
κ_Λ	-0.613	κ_Σ^0	0.79
κ_{Σ^+}	1.45	κ_Σ^-	-0.16
$\kappa_{\Sigma^0\to\Lambda\gamma}$	-1.61		

where Ψ_R is the resonance spinor and $F^{\mu\nu} = \partial^\mu A^\nu - \partial^\nu \mathsf{A}^\mu$. The operator Γ is 1 for the positive parity resonance and $-i\gamma_5$ for the negative parity one.

For spin-$\frac{3}{2}$ resonances, we have used the gauge-invariant effective Lagrangians as discussed in Refs. [56, 64, 65, 77, 78]. We write here the vertex functions used by us in computation involving these vertices. The resonance-nucleon-pion vertex function (e.g.) is given by

$$\Gamma^\alpha_{R_{3/2}\to N\pi} \;=\; \frac{g_1}{m_\pi}\left[\gamma^\alpha (q\cdot p) - \not{p} q^\alpha\right][(1-\chi) + \chi \not{p}/M_p], \tag{A5}$$

and the corresponding electromagnetic vertices are

$$\Gamma^{\alpha\mu}_{R_{3/2}\to N\gamma} = \Big\{(g_2+2g_1)\Big[q^\alpha p^\mu - g^{\alpha\mu}p\cdot q\Big] + g_1\Big[g^{\alpha\mu}\not{p}\not{q} - q^\alpha \not{p}\gamma^\mu + \gamma^\alpha(\gamma^\mu p\cdot q - p^\mu \not{q})\Big] + g_3\Big[(-q^2 g^{\alpha\mu} + q^\mu q^\alpha)\not{p} + (q^2 p^\mu - q^\mu p\cdot q)\gamma^\alpha\Big]\Big\} \times\gamma_5[(1-\chi)+\chi\not{p}/M_p]. \quad \text{(A6)}$$

Here p is the four-momentum of the resonance and q is that of the meson. Index α belongs to the spin-$\frac{3}{2}$ spinor and μ to photon. Interesting property of these vertices is that the product, $p\cdot\Gamma = 0$, where Γ defines the vertices on the left hand side of Eqs. (A.5) and (A.6). As a consequence, the spin-$\frac{1}{2}$ part of the corresponding propagator becomes redundant as its every term is proportional to either p_μ or p_ν. Thus only spin-$\frac{3}{2}$ part of this propagator gives rise to non-vanishing matrix elements.

---

[1] K. G. Wilson, Phys. Rev. **D10**, 2445 (1974).

[2] T. Burch, C. Gattringer, L. Ya. Glozman, C. Hagen, D. Hierl, C. B. Lang, and A. Schäfer, Phys. Rev. D. **74**, 014504 (2006).

[3] D. B. Leinweber, W. Melnitchouk, D. G. Richards, A. G. Williams, and L. M. Zanotti, in *Lattice Hadron Physics*, edited by A. Kalloniatis, D. Leinweber, A. Williams (Springer, Berlin, 2005), P. 71; J. M. Zanotti, B. Lasscock, D. B. Leinweber and A. G. Williams, Phys. Rev. **D71**, 034510 (2005); R.D. Young, D. B. Leinweber, and A. W. Thomas, Phys. Rev. **D71**, 014001 (2005).

[4] S. Capstick and W. Roberts, Prog. Part. Nucl. Phys. **45**, 241 (2000).

[5] U. Löring, K. Kretzschmar, B. C. Metsch, H. R. Petry, Eur. Phys. J A **10**, 395 (201).

[6] M. F. M. Lutz and E. E. Kolomeitsev, Nucl. Phys. **A755**, 29 (2005); J. Hofmann and M. F. M. Lutz, Nucl. Phys. **A763**, 90 (2005); J. Hofmann and M. F. M. Lutz, Nucl. Phys. **A776**, 17 (2006)

[7] M. Benmerrouche, N. C. Mukhopadhyay, J. F. Zhang, Phys. Rev. D **51**, 3237 (1995); N. C. Mukhopadhyay and N. Mathur, Phys. Lett. **B444**, 7 (1998), R. M. Davidson, N. Mathur, N. C. Mukhopadhyay, Phys. Rev. C **62**, 058201 (2000).

[8] R. Workman, R. A. Arndt, I. I. Strakovsky, Phys. Rev. C **62**, 048201 (2000); R. A. Arndt, W. J. Briscoe, I. I. Strakovsky, R. L. Workman, Phys. Rev. C **66**, 055213; Ya. I. Azimov, R. A. Arndt, I. I. Strakovsky, and R. L. Workman, Phys. Rev. C **68**, 045204 (2003); R. A. Arndt, W. J. Briscoe, I. I. Strakovsky, and R. L. Workman, Phys.Rev. C **72**, 058203 (2005).

[9] W. T. Chiang, S. N. Yang, L. Tiator and D. Drechsel, Nucl. Phys. **A700**, 429 (2002).

[10] L. Tiator, D. Drechsel, G. Knöchlein, and C. Bennhold, Phys. Rev. C **60**, 035210 (1999).

[11] D. Drechsel, O. Hanstein, S. S. Kamalov, L. Tiator, Nucl. Phys. **A 645**, 145 (1999)

[12] R. Shyam, Phys. Rev. C **75**, 055201 (2007); R. Shyam, Phys. Rev. C **60**, 055213 (1999); R. Shyam, G. Penner and U. Mosel, Phys. Rev. C **63**, 022202(R) (2001); R. Shyam, Phys. Rev. C **73**, 035211 (2006).

[13] T. Feuster and U. Mosel, Phys. Rev.C **58**, 457 (1998); T. Feuster and U Mosel, Phys. Rev.C **59**,460 (1999).

[14] A. Yu. Korchin, O. Scholten, and R. G. E. Timmermans, Phys. Lett. **B438**, 1 (1998).

[15] G. Penner and U. Mosel, Phys. Rev. C **66**, 055211 (2002); **66**, 055212 (2002); G. Penner, Ph.D. thesis (in English), Universität Giessen, 2002, available at the URL http://theorie.physik.uni-giessen.de

[16] A. Usov and O. Scholten, Phys. Rev. C**72**, 025205 (2005).

[17] V. Shklyar, H. Lenske, U. Mosel, and G. Penner, Phys. Rev. C **71**, 055206 (2005).

[18] A. Usov and O. Scholten, Phys. Rev. C**74**, 015205 (2006).

[19] J. Durand, B. Julia-Diaz, T.-S. H. Lee, B. Saghai, T. Sato, Phys.Rev. C **78**, 025204 (2008).

[20] B. Julia-Diaz, T.-S. H. Lee, A. Matsuyama, T. Sato, L. C. Smith, Phys. Rev. C **77**, 045205 (2008).

[21] B. Julia-Diaz, T.-S. H. Lee, A. Matsuyama, T. Sato, Phys. Rev. C **76**, 065201 (2007).

[22] B. Borasoy, E. Marco, and S. Wetzel, Phys. Rev. C **66**, 055208 (2002).

[23] B. Borasoy, Phys. Rev. D **63**, 094015 (2001); *ibid.*, Eur. Phys. J. A **9**, 95 (2000).

[24] B. Saghai and Z. Li, Eur. Phys. J. A **11**, 217 (2001); Z. Li and B. Saghai, Nucl. Phys. **A644**, 345 (1998).

[25] C. Dover and P. Fishbane, Phys. Rev. Lett. **64**, 3115 (1990).

[26] See, e.g., Z. Papandreou, AIP Conf. Proc, **814**, 453 (2005).

[27] N. Mathur, Y. Chen, S. J. Dong, T. Draper, I. Horvath, F. X. Lee, K. F. Liu, and J. B. Zhang, Phys. Lett. B **605**, 137 (2005)

[28] H. C. Chiang, E. Oset, and L. C. Liu, Phys. Rev. C **44**, 738 (1991).

[29] A. Fix and H. Arenhövel, Phys. Rev. C **66**, 024002 (2002).

[30] Q. Haider and L. C. Liu, Phys. Rev. C **66**, 045208 (2002).

[31] M. Pfeiffer et. al., Phys. Rev. Lett. **92**, 252001 (2004).

[32] A. Sibirtsev, J. Haidenbauer, J. A. Niskanen, and Ulf-G. Meissner, Phys. Rev. C **70**, 047001 (2004).

[33] G. Knöchlein, D. Drechsel, and L. Tiator, Z. Phys. A **352**, 327 (1995).

[34] J. W. Price *et al.*, Phys. Rev. C **51**, R2283 (1995).

[35] B. Krusche *et al.*, Phys. Rev. Lett. **74**, 3736 (1995).

[36] J. Ajaka *et al.*, Phys. Rev. Lett. **81**, 1797 (1998).

[37] A. Bock *et al.*, Phys. Rev. Lett. **81**, 534 (1998).

[38] R. Thompson *et al.*, Phys. Rev. Lett. **86**, 1702 (2001).

[39] M. Dugger *et al.*, Phys. Rev. Lett. **89**, 222002 (2002).

[40] F. Renard *et al.*, Phys. Lett. B528, 215 (2002).

[41] V. Crede *et al.*, Phys. Rev. Lett. **94**, 012004 (2005).

[42] O. Bartholomy *et al.*. Eur. Phys. J. **33**, 133 (2007).

[43] D. Elsner *et al.*, Eur. Phys. J. **33**, 147 (2007).

[44] O. Bartalini *et al.*, Eur. Phys. J. **33**, 169 (2007).

[45] B. Krusche and S. Schadmand, Prog. Part. Nucl. Phys. **51**, 399 (2003).

[46] A. V. Anisovich, A. Sarantsev, O. Bartholomy, E. Klempt, V. A. Nikonov, and U. Thoma, Eur. Phys. J. A **25**, 427 (2005).

[47] P. Hoffmann-Rothe *et al.*, Phys. Rev. Lett. **78**, 4697 (1997).

[48] J. Weiss *et al.*, Eur. Phys. A **11**, 371 (2001).

[49] J. Weiss *et al.*, Eur. Phys. A **16**, 275 (2003).

[50] V. Kuznetsov *et al.*, Phys. Lett. **B647**, 23 (2007).

[51] I. Jaegle *et al.*, arXiv:0804.4841.

[52] V. Shklyar, H. Lenske, and U. Mosel, Phys. Lett. **B650**, 172 (2007).

[53] A. Fix, L. Tiator and M. V. Polyakov, Eur. Phys. J. A **32**, 311 (2007).

[54] O. Scholten, S. Kondratyuk, L. Van Daele, D. Van Neck, M. Waroquier and A.Yu. Korchin, Acta Phys. Pol.**B33**, 847 (2002).

[55] R.G. Newton, *Scattering theory of Waves and Particles* (Springer, New York, 1982).

[56] S. Kondratyuk and O. Scholten, Nucl. Phys. **A677**,396 (2000); S. Kondratyuk and O. Scholten, Phys. Rev. C **62**, 025203 (2000).

[57] S. Kondratyuk and O. Scholten, Phys. Rev. C **65**, 038201; *ibid.* Phys. Rev. C **64**, 024005 (2001)

[58] A.Yu. Korchin and O.Scholten, Phys. Rev. C **68**, 045206 (2003).

[59] T. Sato and T.-S. H. Lee, Phys. Rev. C **54**, 2660 (1996)

[60] W. T. Chiang, B. Saghai, F. Tabakin, T.-S. H. Lee, Phys. Rev. C **69**, 065208 (2004).

[61] M.F.M. Lutz and E.E. Kolomeitsev, Nucl. Phys. **A700**, 193 (2002).

[62] S. Kondratyuk, K. Kubodera, F. Myhrer and O.Scholten, Nucl. Phys. A736, 339 (2004).

[63] V. Shklyar, G. Penner and U. Mosel, Eur. Phys. J A21, 445 (2004).

[64] V. Pascalutsa, Nucl. Phys. **A680**, 76 (2000).

[65] V. Pascalutsa, Phys. Lett. **B503**, 85 (2001).

[66] W. M. Yao *et al.* (Particle Data Group), J. Phys. G: Nucl. Part. Phys. **33**, 1 (2006).

[67] I.J. General and S.R. Cotanch, Phys. Rev. C **69**, 035202 (2004).

[68] R. M. Davidson and R. Workman, Phys. Rev. C **63**, 025210 (2001).

[69] V. A. Trysuchev, Eur. Phys. J. A **22**, 97 (2004).

[70] K. Nakayama, Y. Oh, H. Haberzettl, arXiv:0803.3169.

[71] Virginia Tech SAID data base, see the URL http://gwdac.phys.hwu.edu/, FA08 solution R. A.Arndt, I. I. Strakovsky, and R. L. Workman, Phys. Rev. C **53**, 430 (1996); R. A. Arndt, W. J. Briscoe, I. I. Strakovsky and R. L. Workman, Phys. Rev. C **74**, 045205 (2006).

[72] Jun He, B. Saghai and Zhenping Li, Phys. Rev. C **78**, 035204 (2008).

[73] C. Sauermann, B. L. Friman, and W. Nörenberg, Phys. Lett. B **341**, 261 (1995); C. Deutsch-Sauermann, B. Friman, and W. Nörenberg, *ibid.* 409, 51 (1997).

[74] L. Tiator, C. Bennhold, and S. S. Kamalov, Nucl. Phys. A580, 455 (1994).

[75] N. C. Mukhopadhyay, J. F. Zhang, and M. Benmerrouche, Phys. Lett. **B364**, 1 (1995).

[76] J. D. Bjorken and S. D. Drell, *Relativistic Quantum Mechanics* (McGraw-Hill, New York, 1964).

[77] V. Pascalutsa, Phys. Rev. D **58**, 096002 (1998).

[78] L. Jahnke and S. Leupold, Nucl. Phys. **A778**, 63 (2006).